Magnetic properties of the Old Crow tephra: Identification of a complex iron titanium oxide mineralogy

France Lagroix, Subir K. K. Banerjee, Mike. J. Jackson

Magnetic properties of the Old Crow tephra: Identification of a complex iron titanium oxide mineralogy

France Lagroix, Subir K. Banerjee, and Mike J. Jackson

Institute for Rock Magnetism, Department of Geology and Geophysics, University of Minnesota, Minneapolis, Minnesota, USA

Received 8 July 2003; revised 20 October 2003; accepted 23 October 2003; published 16 January 2004.

[1] The mineralogy and grain-size distribution of the Fe-Ti oxide population of the Old Crow tephra bed, outcropping at the Halfway House loess deposit in central Alaska, are characterized through multiple low- and high-temperature magnetization experiments. The characterization is facilitated by heavy liquid separation of the bulk sample into a low-density (<2850 kg/m^3, LD) and high-density (≥2850 kg/m^3, HD) fraction. Three phases of the magnetite-ulvöspinel solid solution series, $Fe_{3-x}Ti_xO_4$, $x = 0$, 0.1, and 0.3 are identified along with one phase of the ilmenite-hematite solid solution series, $Fe_{2-y}Ti_yO_3$, $y = 0.83$. All four phases are present in both density separates, where coarser grains dominate the HD sample and finer more oxidized grains dominate in the LD sample. Low-temperature frequency dependence and field dependence of both the in-phase and quadrature components of magnetic susceptibility are found particularly useful in identifying the magnetic ordering temperature of titanohematite phases with $y > 0.8$ and may play an equally important role as magnetic indicator of titanomagnetite. Furthermore, we demonstrate the ability of low-temperature magnetism to locate a 1 mm thick tephra bed dispersed in loess over 10 cm depth, through the identification of very low concentrations of a titanohematite phase with $y = 0.9$. The potential for advancing regional correlation of sedimentary deposits through the identification of Fe-Ti oxides common to tephra beds by low-temperature magnetism is illustrated in this study. *INDEX TERMS:* 1540 Geomagnetism and Paleomagnetism: Rock and mineral magnetism; 1512 Geomagnetism and Paleomagnetism: Environmental magnetism; 1519 Geomagnetism and Paleomagnetism: Magnetic mineralogy and petrology; 8404 Volcanology: Ash deposits; 5109 Physical Properties of Rocks: Magnetic and electrical properties; *KEYWORDS:* low-temperature magnetism, frequency and amplitude dependence of AC susceptibility, ilmenite-hematite and magnetite-ulvospinel solid solution series, tephra, stratigraphic correlation

Citation: Lagroix, F., S. K. Banerjee, and M. J. Jackson (2004), Magnetic properties of the Old Crow tephra: Identification of a complex iron titanium oxide mineralogy, *J. Geophys. Res.*, *109*, B01104, doi:10.1029/2003JB002678.

1. Introduction

[2] Tephra deposits are key indicator beds facilitating stratigraphic correlations and chronology in various depositional environments (i.e., marine, lacustrine, terrestrial). In eastern Beringia, the geographic region encompassing Alaska and the Yukon Territory, tephra beds whose provenance includes the volcanic fields of the Aleutian Arc, Alaskan Peninsula, Cook Inlet and Wrangell mountains, have been deposited since the Miocene epoch [*Fournelle et al.*, 1994; *Miller and Richter*, 1994; *Plafker and Berg*, 1994]. *Westgate* [1982] and *Westgate et al.* [1985] investigated the regional extent of the Old Crow (OC) tephra deposit, where the total volume of tephra ejected probably exceeded 50 km^3. The OC tephra was deposited 140,000 ± 10,000 years ago [*Berger et al.*, 1992; *Westgate et al.*, 1990] over most of Alaska and western Yukon and there are at least 15 known localities where it crops out [*Hamilton and Brigham-Grette*, 1991; *Westgate et al.*, 1985]. Preservation of the tephra bed, in numerous locations, is in part due to the nonglaciated state of central Alaska during the Last Glacial Maximum and previous Pleistocene glacial advances. In eastern Beringia, the OC tephra represents the most widespread petrostratigraphic marker and has been indispensable to geoscientists reconstructing the regional paleoclimate and paleoenvironment.

[3] A recent report suggests the Dawson tephra, found in the Klondike region of the Yukon, may be as significant in volume and regional coverage as the OC tephra; however, its distribution is currently not well known [*Froese et al.*, 2002]. In the Fairbanks area alone, there are 19 distinct tephra beds, four of which are reported to crop out within a ~12 m loess-paleosol deposit at the Halfway House site located ~50 km west of Fairbanks along the Parks Highway [*Preece et al.*, 1999]. Other published stratigraphies of the loess-paleosol deposit at Halfway House only identify one tephra bed, the OC tephra [*Begét*, 1990; *Begét and Hawkins*, 1989; *Begét et al.*, 1990; *Lagroix and Banerjee*, 2002; *Oches et al.*, 1998]. Tephra beds that are thin,

0148-0227/04/2003JB002678$09.00

Table 1. Specific Gravity of Mineral Series End-Members Within the Old Crow Tephra[a]

	Specific Gravity, kg/m^3
Volcanic glass	2300–2900
Plagioclase	
Albite	2630
Anorthite	2760
Orthopyroxene	
Enstatite	3200
Ferrosilite	3950
Clinopyroxene	
Augite	2960
Titanomagnetite	
Magnetite	5200
Ulvöspinel	4780
Titanohematite	
Ilmenite	4720
Hematite	5250

[a]From *Deer et al.* [1966] and *Lide* [2002].

discontinuous or dispersed due to local deformation are difficult to identify visually in the field. Fortunately, the mineralogy of tephra material tends to be quite different from the sediment in which it is found, allowing for the identification of expected tephra-associated minerals through laboratory experiments.

[4] We present, herein, a detailed analysis of the mineralogy and grain-size distribution of the Fe-Ti oxide fraction of the OC tephra sampled at Halfway House with low- and high-temperature magnetization experiments. Beyond assessing the bulk composition, we wish to determine if the mineralogy and grain-size distribution of the Fe-Ti oxides within the matrix versus within the glass shards as inclusions is homogeneous. Finally, we will demonstrate that our rock magnetic approach has the potential of identifying tephra beds that are otherwise not identified.

2. Bulk Composition of the Old Crow Tephra at Halfway House

[5] *Westgate et al.* [1985] determined from geochemical and electron microprobe analysis that the OC tephra is a two-pyroxene calc-alkaline dacite with dacitic to rhyolitic clear bubble-wall glass shards. The mineralogical assemblage is composed, predominantly, of hypersthene, augite, plagioclase, titanomagnetite and ilmenite [*Westgate et al.*, 1985]. Furthermore, from energy-dispersive microprobe analysis they determined that the titanomagnetite ($Fe_{3-x}Ti_xO_4$) population (from 17 grains) has an average composition of 28 mol.% ulvöspinel (TM28, $x = 0.28$) and that the ilmenite population (from 13 grains) has an average composition of 17 mol.% hematite corresponding to a titanohematite ($Fe_{2-y}Ti_yO_3$) with 83% ilmenite (TH83, $y = 0.83$).

3. Experimental Approach: Heavy Liquid Separation

[6] The great disparity between the specific gravity of volcanic glass and Fe-Ti oxides allows for density separation isolating the mineral population from the glass shards. Specific gravity ranges of minerals found in the OC tephra are listed in Table 1. A sample of the bulk OC tephra was separated into a low-density (LD) and high-density (HD) fractions using the LST Heavy Liquid purchased from Central Chemical Consulting Pty. Ltd (Karrinyup, Western Australia). The heavy liquid is a solution of lithium heteropolytungstates in water, which at room temperature has a specific gravity of 2850 kg/m^3. The bulk sample was permitted to settle for a period of 24 hours. Mineral grains with a specific gravity less than the heavy liquid would float, grains with a specific gravity equal to the heavy liquid would stay in suspension and those with a specific gravity greater than the heavy liquid would settle following Stokes' law. The settled and suspended materials are incorporated within the HD fraction while the floating material forms the LD fraction. Furthermore, a mineral such as plagioclase, if containing Fe-Ti oxide inclusions increasing the grain's specific gravity, could very well settle and be found in the HD fraction. Under transmitted light we could ascertain that the separated LD fraction is composed of mostly glass shards and plagioclase with minor amounts of small euhedral opaque minerals. The separated HD fraction is composed of large subhedral to anhedral opaque minerals, orthopyroxene and clinopyroxene with minor amounts of plagioclase and apatite.

[7] The sample mass of the bulk, LD, and HD samples is 188, 241, and 27.5 mg, respectively. Hysteresis loops and their derived parameters demonstrate that the LD and HD fractions are representative of the bulk sample (Figure 1 and Table 2). We can estimate the fraction of HD and LD within the bulk sample with magnetic parameters that should be linearly additive such as saturation and remanent magnetization. The fraction x of HD within the bulk sample is

$$x = \frac{P_{\mathrm{Bulk}} - P_{\mathrm{LD}}}{P_{\mathrm{HD}} - P_{\mathrm{LD}}}, \tag{1}$$

where P is the magnitude of the linearly additive magnetic parameter. Using equation (1) with the saturation magnetization, M_S, values listed in Table 2, the HD sample represents 0.62% of the bulk sample mass. The same exercise using

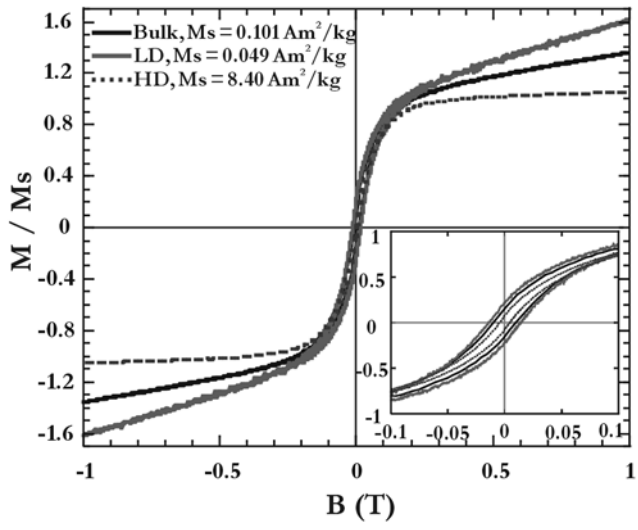

Figure 1. Hysteresis loops of the low-density (LD) and high-density (HD) samples separated from the bulk sample uncorrected for the high-field paramagnetic contribution. For ease of comparison the loops are normalized to their saturation magnetization (M_S) determined after the high-field slope correction. Inset shows an enlarged view of the data near the origin.

Table 2. Room Temperature Hysteresis Loop Derived Parameters

	Bulk	High-Density Fraction $\rho \geq 2850$ kg/m^3	Low-Density Fraction $\rho < 2850$ kg/m^3
M_S, A m^2/kg	1.01×10^{-1}	8.40×10^{0}	4.91×10^{-2}
M_R, A m^2/kg	1.55×10^{-2}	6.38×10^{-1}	1.08×10^{-2}
B_C, mT	10.2	4.46	14.4
B_{CR}, mT	31.0	18.3	35.4
M_R/M_S	0.154	0.076	0.220
B_{CR}/B_C	3.04	4.09	2.47
High-field slope χ_{HF}, m^3/kg	4.51×10^{-8}	5.59×10^{-7}	3.78×10^{-8}

other mass normalized magnetic parameters measured both at room temperature and across a low temperature range yields HD fractions between 0.5% and 1.5% of the bulk sample mass.

[8] In order to achieve one of our goals of fully characterizing the magnetic mineralogy, the grain size and how these are distributed within the LD and HD fraction the three samples mentioned above (bulk, LD and HD) were subjected to low-temperature remanence and induced (alternating low and direct high fields) magnetization experiments. Furthermore, resolving the complex magnetic mineralogy was also assisted by high temperature magnetometry on an additional bulk sample of the OC tephra (~65 mg).

4. Magnetic Characterization of the Old Crow Tephra at Halfway House

4.1. Observations

4.1.1. High-Temperature Thermomagnetic Experiment

[9] The high-temperature thermomagnetic experiment was conducted on a Princeton Measurements Vibrating Sample Magnetometer outfitted with a flowing helium gas furnace. The magnetization was induced in a 1 Tesla magnetic field and measured at a 1°C interval on heating from 25°C to 700°C as well as on cooling back to 25°C in order to assess any mineralogical alteration incurred during

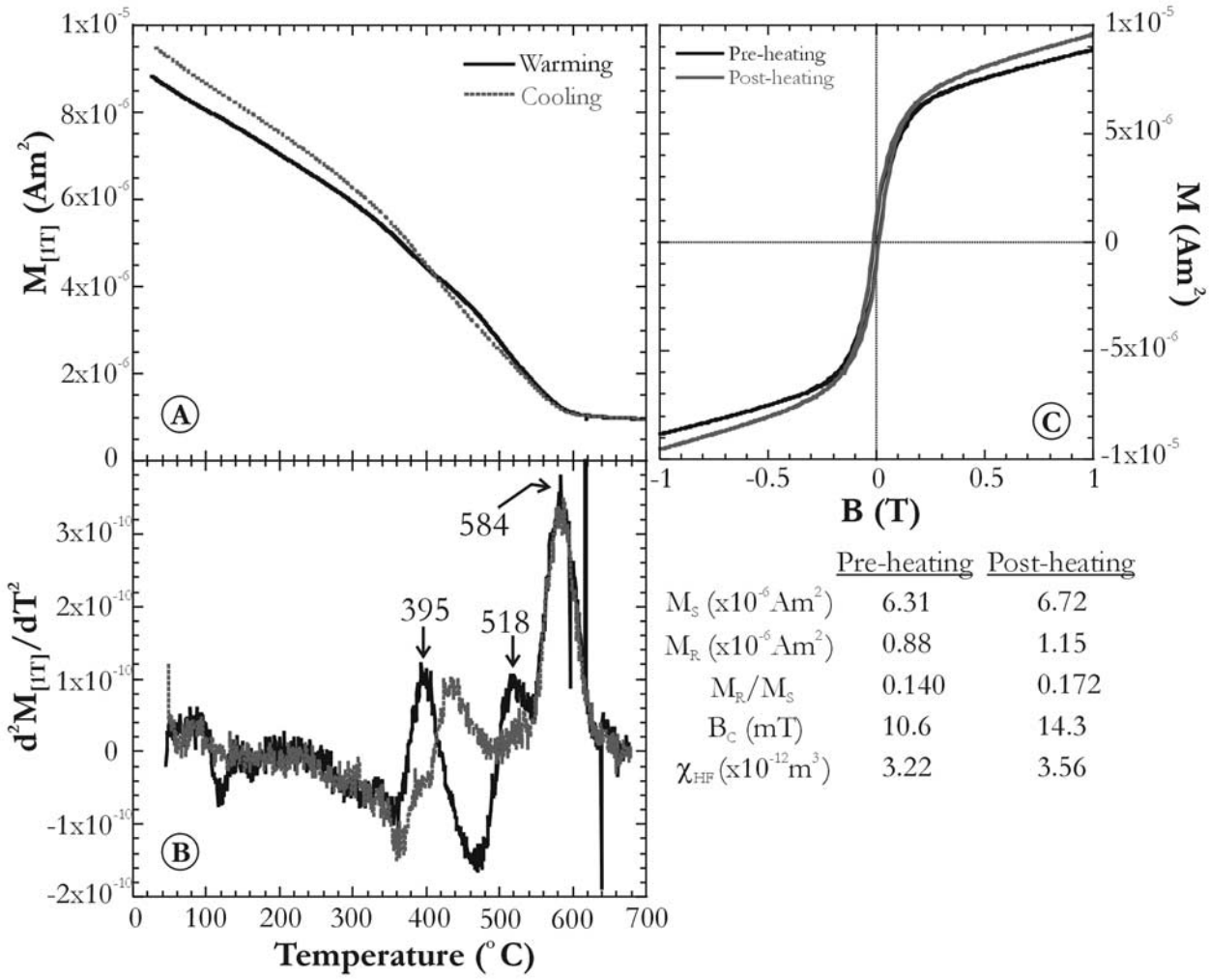

Figure 2. High-temperature dependence of the bulk sample's (~65 mg) magnetization induced in a 1 T magnetic field. (a) Measured magnetization upon warming from 25°C to 700°C and cooling back to room temperature. (b) Second derivative of the measured magnetization identifying the Curie temperatures of three magnetite-ulvöspinel series phases. (c) Hysteresis loop and its derived parameters of the bulk sample before and after the thermomagnetic experiment.

heating (Figure 2a). More commonly used methods for T_C determination from thermomagnetic experiments are not adequate here [*Ade-Hall et al.*, 1965; *Grommé et al.*, 1969; *Moskowitz*, 1981] because of the multiple ferrimagnetic mineral phases. Instead, the M_{1T}(T) was smoothed with a 20 points (20°C) running average before calculating the first derivative of the M_{1T}(T). The dM_{1T}/dT data was also smoothed with a 20 points running average before calculating the second derivative. The smoothing filters out short wavelength fluctuations caused by instrumental noise, while longer wavelength variations produced by the sample remain. The maxima, in the second derivative, highlight points of maximum curvature in the induced magnetization data, which correspond to Curie temperatures, T_C (Figure 2b). T_C are observed at 395°C, 518°C, and 584°C. The preheating and postheating hysteresis loops (Figure 2c) indicate that the sample suffered minor alteration indicated by increases in saturation and remanent magnetization as well as coercivity. Our interpretations of the observed T_C and minor alteration incurred will be discussed in section 4.2.2.

4.1.2. Low-Temperature Frequency and Field Dependence of AC Susceptibility

4.1.2.1. In-Phase Susceptibility

[10] The AC susceptibility frequency and field dependence experiments were conducted on Quantum Designs' Magnetic Property Measurement System (MPMS) over the temperature range of 10 to 300 K at 10 K measuring steps. The in-phase and quadrature components of susceptibility (χ' and χ'') of the bulk, LD and HD samples were measured in a constant 240 A/m field at seven frequencies (1, 3, 10, 30, 100, 300, and 1000 Hz) (Figure 3; only 1, 10, 100, and 1000 Hz data are shown). Subsequently, χ' and χ'' of the bulk sample were measured in three variable field amplitudes (80, 160, and 240 A/m) at a constant 100 Hz frequency (Figure 4). The complexity of the results arises from the varying magnetic behaviors (paramagnetism, antiferromagnetism, and ferrimagnetism) of multiple mineral phases and grain sizes.

[11] The in-phase susceptibility data (Figure 3 (left), $\chi'(f, T)$; and Figure 4 (left), $\chi'(H, T)$) exhibits similar features but at different amplitudes in all three samples. Between 10 and 30 K we can observe a large decrease in χ' in the bulk and LD samples but not in the HD sample, which confirms that most ferromagnetic (broadly speaking) minerals were separated into the high-density fraction. Furthermore, removing the paramagnetic component from the bulk sample $\chi'(f, T)$ data, by calculating the Curie constant from the high-field M(H) slope at 10 K, yields a $\chi'(f, T)$ function (not shown) comparable in form to the HD sample. The increase in χ' between 30 and 90 K, for the bulk and HD samples, is accompanied by an increasing frequency dependence (χ'_{fd}), seen in all three samples, which reaches a maximum at 60 K for the lowest frequencies and at progressively higher temperature with increasing frequency (Figure 5a). The maximum χ'_{fd}, in this temperature range, is the largest and forms the sharpest peak in HD (up to ~16%) and is the lowest and forms the most rounded peak in LD (up to ~4%). From 10 to 90 K, χ' is independent of the applied field (Figure 5b). Between 90 K and 210 K, χ' continues to increase at a slower rate. χ'_{fd} is constant with a slight tendency to increase with increasing temperature (especially for LD) and low remaining below 2% between 90 and 300 K. Furthermore, we observe a continuous increase in the field dependency of χ'. χ' reaches a maximum at 210 K before decreasing rapidly (210 to 230 K), stabilizing and increasing slightly up to 300 K. Interpretations are presented in section 4.2.

4.1.2.2. Quadrature Susceptibility

[12] Three physical properties may cause a sample to exhibit significant quadrature susceptibility (χ''). These are electrical conductivity, time-dependent viscous behavior and low-field hysteresis. The χ'' resulting from both conductivity and viscosity (magnetic relaxation) will exhibit frequency dependence, while that resulting from low-field hysteresis will show amplitude dependence [*Jackson et al.*, 1998]. Furthermore, we can quantify the magnitude of χ'' due to magnetic relaxation from *Néel*'s [1949] single-domain theory and its derivations presented by *Mullins and Tite* [1973], with

$$\chi''[\text{viscosity}] = -\frac{\pi}{2}\frac{\Delta\chi'}{\Delta \ln f}, \tag{2}$$

where f represents the measuring frequencies (at least one order of magnitude difference) and χ' is the in-phase susceptibility measured at the corresponding frequencies. There is no evidence for conductive minerals, such as iron sulfides, in our samples and magnetite even though present does not have high conductivity below 120 K.

[13] The quadrature component of the $\chi(f, T)$ experiment (Figure 3, right) mimics the magnetic relaxation features observed in Figure 5a with the notable addition of a frequency-independent peak in χ'' at 190 K. The lower temperature maximum in χ'' moves to a higher temperature and has a larger magnitude with increasing frequency while the higher temperature peak in χ'' is constantly at 190 K independent of frequency and increases in magnitude with decreasing frequency. When varying the amplitude of the field the low temperature peak in χ'' occurs at a constant temperature, 80 K, while its magnitude increases with increasing applied field (Figure 4, right). The high-temperature peak in χ'' also increases in magnitude with increasing applied field, but the temperature at which the peak occurs decreases slightly or remains constant with increasing field amplitude. When applying equation 2 (open symbol data in Figure 3 (right)), we can observe that the quadrature susceptibility is entirely due to magnetic relaxation below 70 K. Above 70 K, susceptibility varies with field amplitude due to titanomagnetite and titanohematite phase(s) exhibiting low-field hysteresis, and magnetic relaxation cannot account for all of the χ'' variation (see discussion in section 4.2). Following the peak at 190 K, the hysteretic behavior of the titanohematite phase is lost by 220 K. Above 220 K, magnetic relaxation can account for almost all of χ'' while the small amount of low-field hysteresis is due to the titanomagnetite phases.

4.1.3. Low-Temperature and High-Field Experiments

[14] High-field induced magnetization experiments were conducted on all three samples using the Quantum Designs MPMS. The samples were subjected to a 1 and 2.5 Tesla field while the induced magnetization was measured at a 5 K (5°C) interval on warming from 10 to 300 K (Figure 6a). Unlike in the low-field experiments, the high-field results

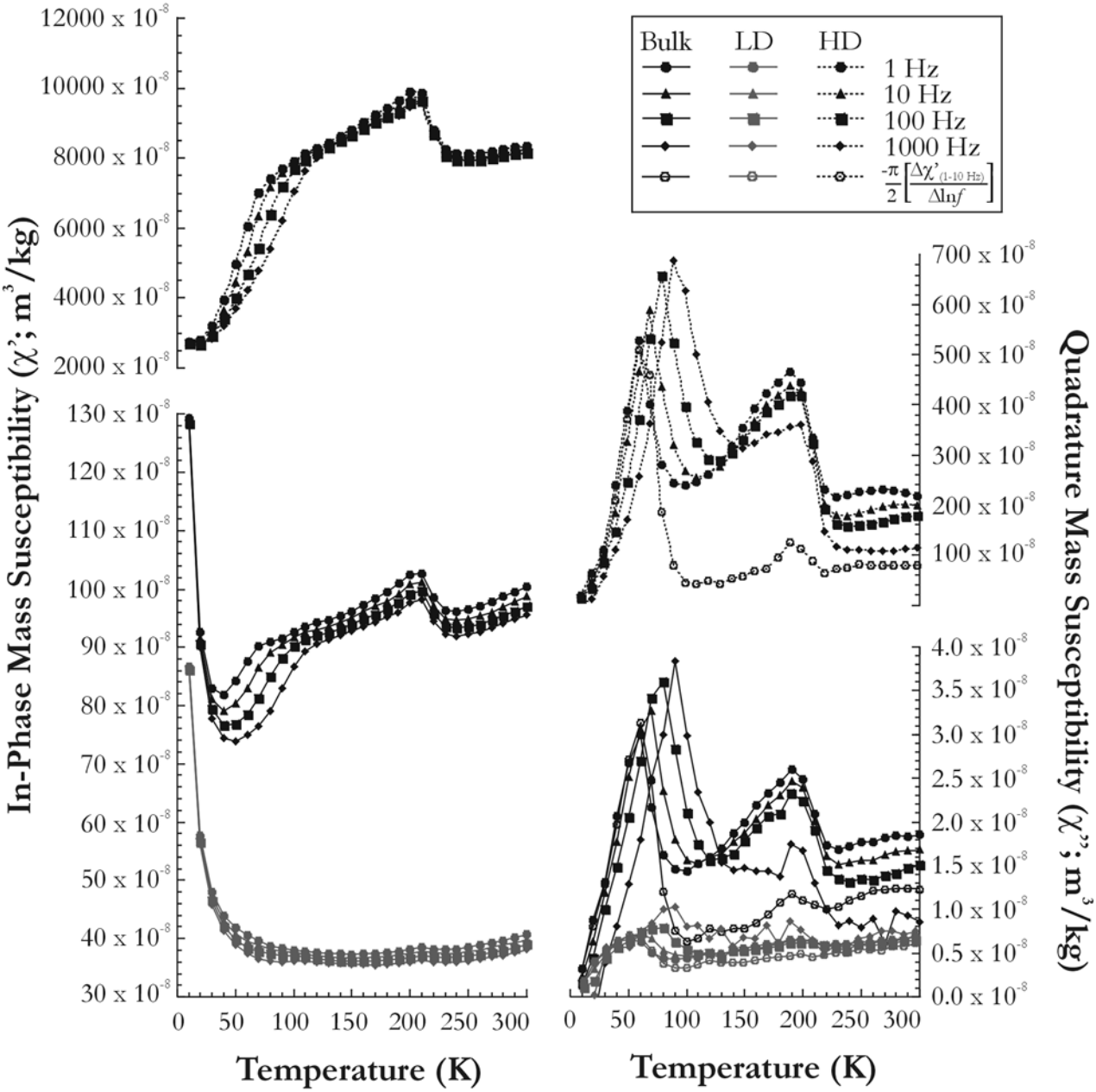

Figure 3. (left) In-phase and (right) quadrature components of magnetic susceptibility measured between 10 K and 300 K in a constant 240 A/m field amplitude and at seven frequencies (1, 3, 10, 30, 100, 300, and 1000 Hz; not all shown) for the bulk, LD, and HD samples. Note the break in the *y* axis scale for both the in-phase susceptibility and quadrature susceptibility.

show no visible magnetic ordering transition in the region of 200 K. However, the first derivative of the HD sample data (Figure 6b) does indicate a change in slope at 230 K in both fields, with a smaller change in slope at the higher field. The transition is not evident in the LD and bulk samples, most likely due to a swamping by the paramagnetic signal, which increases linearly with increasing applied field. Only in the HD sample where the Fe-Ti oxides have been preferentially concentrated do we observe an increase in induced magnetization at 230 K, a temperature coincident with the transition of the titanohematite phase to its paramagnetic state.

[15] We can calculate the high-field susceptibility (χ_{HF}) from the data in Figure 6a and plot its reciprocal against temperature (Figure 7a). To assess the linearity of M(H) multiple field steps up to 5 T for the bulk sample and 2.5 T for the LD and HD samples were measured at 10 K only (not shown), where saturation would be the most difficult. Linear fit correlation coefficients (R^2) for the bulk, LD, and HD samples were 0.9991, 0.9991, and 0.9975, respectively, providing satisfactory evidence that saturation was achieved and therefore should be achieved at higher temperatures justifying the use of only two data points (i.e., M(1T) and M(2.5T)) to determine the temperature dependence of χ_{HF} from 10 to 300 K. Once again the LD and bulk samples appear to be dominated by the paramagnetic fraction, indicated by the linearity of $1/\chi_{HF}$, while the HD sample

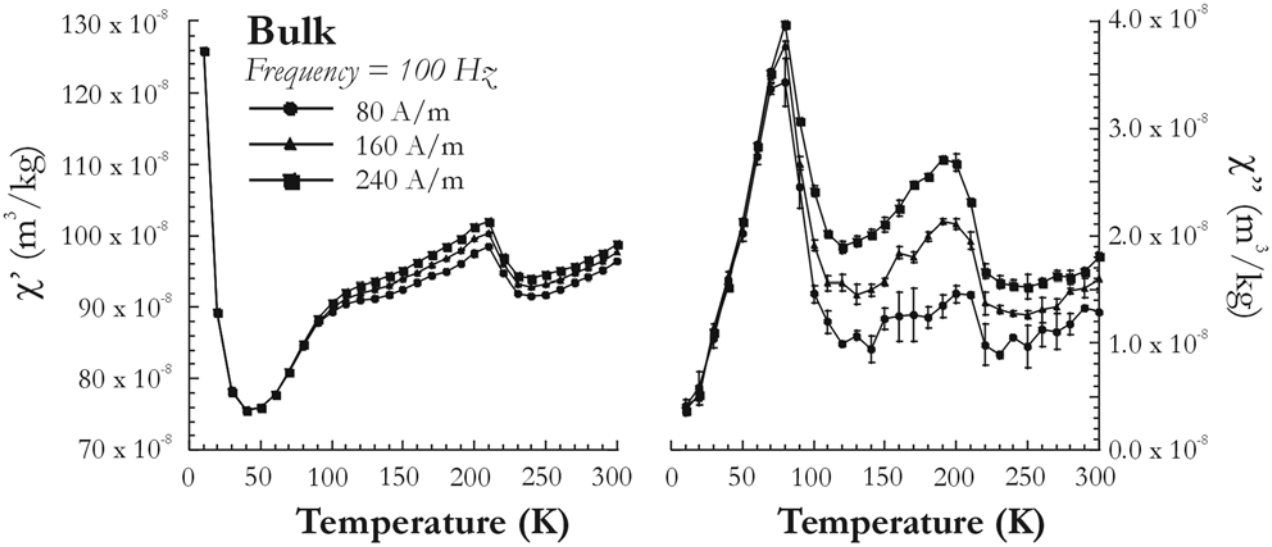

Figure 4. (left) In-phase and (right) quadrature components of magnetic susceptibility measured between 10 K and 300 K at a constant 100 Hz frequency and in three variable field amplitudes (80, 160, and 240 A/m) for the bulk sample.

clearly demonstrates the magnetic disordering transition to paramagnetism of the titanohematite phase occurring at ~230 K. The first derivative of the $1/\chi_{HF}$ data (Figure 7b) provides the only evidence of this magnetic ordering in the bulk sample in high-field experiments. In agreement with the HD sample, the transition in high fields, although not sharply defined appears to occur at 230 K instead of 210 K or 220 K as observed in the $\chi'(f, T)$ and $\chi''(f, T)$ data, respectively, perhaps due to the persistence of short-range ordering in high fields.

4.1.4. Low-Temperature Remanence Experiments

[16] We conducted two saturation isothermal remanent magnetization (SIRM) experiments on all three samples using the MPMS SQUID magnetometer. The first experiments investigated the behavior of an SIRM acquired at low temperature (i.e., 10 K; LT-SIRM), while in the second experiment we would observe the behavior of an SIRM acquired at room temperature (i.e., 300 K; RT-SIRM) when cycled through a range of low temperatures.

[17] Figure 8a plots the data of the LT-SIRM experiments where the sample treatment begins at 300 K and is cooled to 10 K in a zero magnetic field (ZFC). An SIRM is acquired in a 2.5 T field before it is switched off and the remanence measured on warming back to 300 K. A 2.5 T magnetic field is switched on again at 300 K and the sample is cooled back to 10 K in the magnetic field (FC). At 10 K the field is switched off and remanence is measured on warming back to 300 K. In all three samples the loss of remanence on warming is the same whether the sample was ZFC or FC. The initial remanence at 10 K of the HD sample is 2 orders of magnitude greater than that of the bulk or LD samples (note the two y axes scales in Figure 8a); however, the HD sample undergoes the greatest remanence loss on warming. The first derivative of ZFC and FC data (not shown) indicates a change in the rate of remanence loss at 65 K at which point the LD, bulk, and HD samples have already lost 26%, 44%, and 77%, respectively, of their LT-SIRM. Only the HD sample exhibits a second remanence loss rate change near magnetite's Verwey transition ($T_V \sim 122$ K). At 300 K the total remanence loss is 56%, 68%, and 92% for the LD, bulk, and HD samples, respectively. No anomaly is observed in the vicinity of the magnetic ordering of the titanohematite phase.

[18] Figure 8b plots the behavior of the RT-SIRM experiment where an SIRM is acquired in a 2.5 T magnetic field at 300 K and remanence is measured on cooling to 10 K and

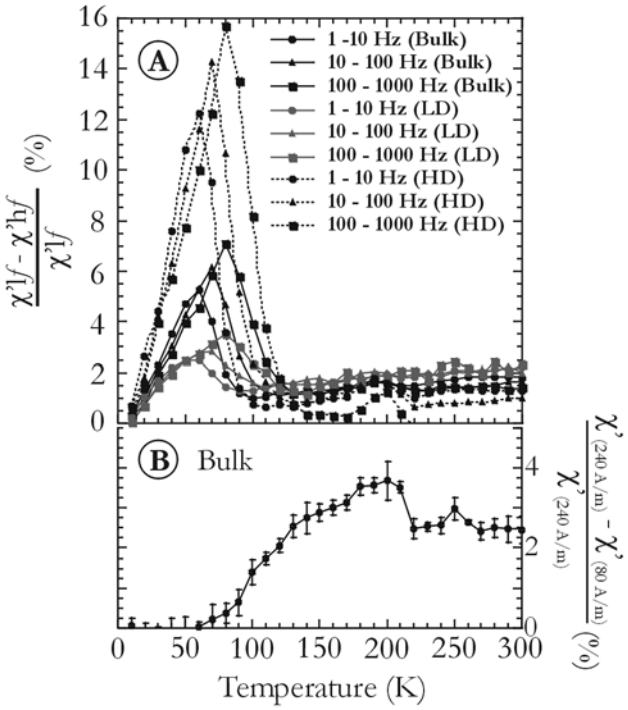

Figure 5. (a) Frequency dependence between 1 and 10 Hz, 10 and 100Hz, and 100 and 1000 Hz of the bulk, LD, and HD samples' in-phase susceptibility data shown in Figure 3. (b) Field dependence between 80 and 240 A/m of the bulk sample's in-phase susceptibility data shown in Figure 4.

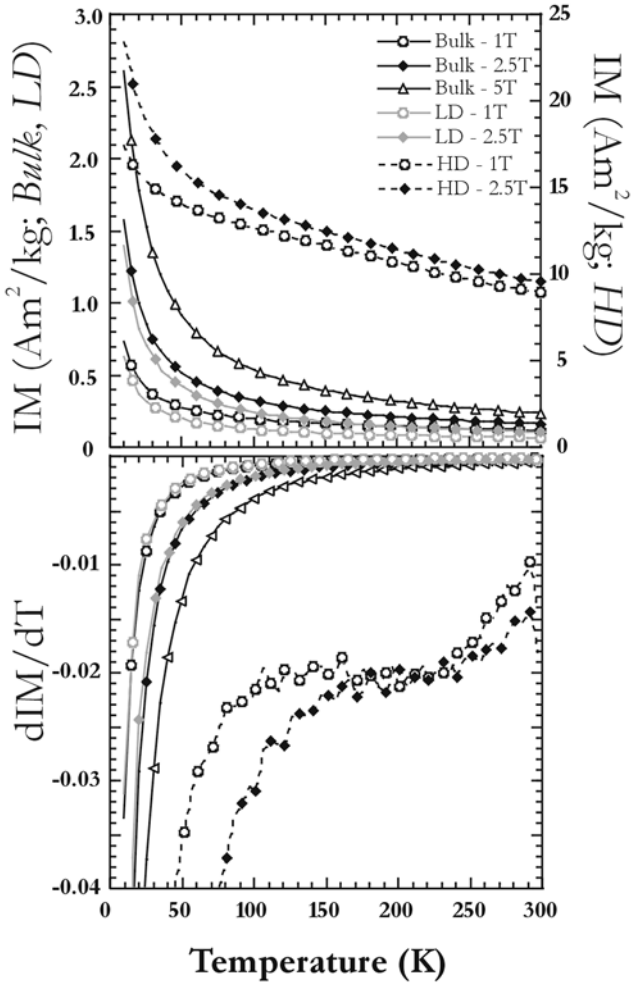

Figure 6. (top) Induced magnetization (IM) in 1 and 2.5 T for the bulk, LD and HD samples and in 5 T for the bulk sample across the 10 K to 300 K temperature range. Note the two *y* axes: left is for the bulk and LD samples magnetization and right is for the HD magnetization. (bottom) First derivative of the 1 and 2.5 T induced magnetization for the bulk, LD, and HD samples.

warming back to 300 K. This is the only experiment where all three samples exhibit changes at T_V. All three samples undergo a loss of remanence through T_V on cooling from room temperature. Both the bulk and LD samples show a slight (<3%) initial increase in remanence before going through T_V but upon reaching 10 K the bulk, LD and HD samples have lost 10%, 3% and 40% of their initial room temperature remanence. On warming back to 300 K the remanence is reversible up to 50 K. All three samples show limited, 1–3%, recovery on warming through T_V, but this is short-lived. Total remanence losses after a full cooling-warming cycle are 14%, 9%, and 40% for the bulk, LD, and HD samples, respectively.

4.2. Interpretation of Observations

[19] The various high- and low-temperature experiments presented in this paper independently confirm the mineralogical work by *Westgate et al.* [1985] that TM28 and TH83 dominate the magnetic mineralogical assemblage of the Old Crow tephra outcropping at the Halfway House site in central Alaska. However, our experiments have enabled us to sample a larger population of Fe-Ti oxide grains than is usually achievable by microprobe analysis resulting in the identification of three magnetite-ulvöspinel solid solution series compositions (see section 4.2.2) and a titanium-rich ilmenite-hematite solid solution series composition (see section 4.2.1). Furthermore, the density separation approach allowed further isolation of the Fe-Ti oxides, of which the (titano)magnetite phases constitute only 0.11% to 0.17% of a bulk sample (see section 4.2.2). The results presented in section 4.1 also suggest that all the Fe-Ti oxide phases are present in both the LD and HD fractions.

4.2.1. Titanohematite Phase

[20] The frequency-independent (but field-dependent) peaks in χ' at 210 K and χ'' at 190 K are attributed to a titanium-rich phase of the ilmenite-hematite series undergoing a change in magnetic ordering to paramagnetism above these temperatures. The magnetic properties of the hematite-ilmenite series phases are strongly dependent on the titanium content. The simplest yet most robust equation relating composition and Curie or Néel temperatures, given the two end-members, was deduced by *Nagata and Akimoto* [1956]:

$$T_C \text{ or } T_N(^\circ\text{C}) = 675 - 885y, \tag{3}$$

where y ($0 \leq y \leq 1$) in $y\text{FeTiO}_3 \cdot (1-y)\alpha\text{Fe}_2\text{O}_3$ represents the molar fraction of ilmenite (i.e., proportion of the

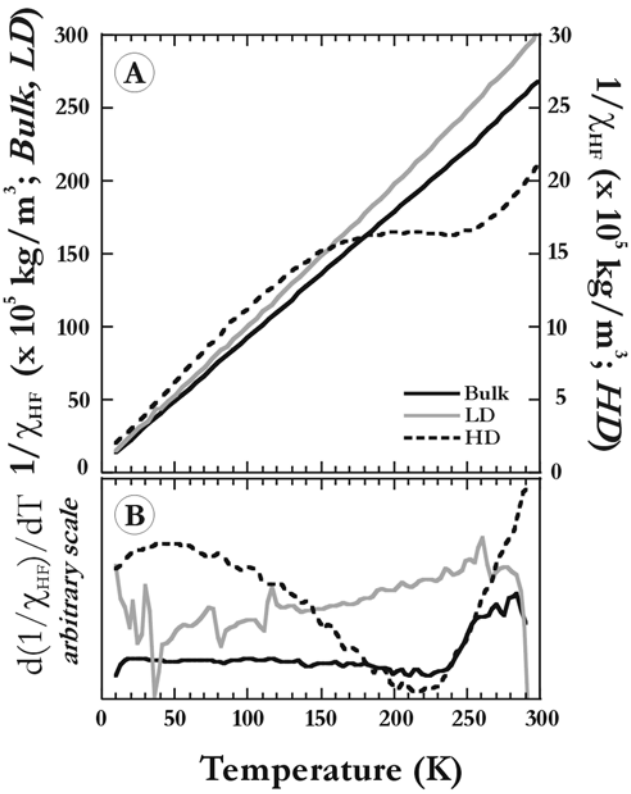

Figure 7. (a) Reciprocal of the high-field susceptibility (χ_{HF}) for the bulk, LD, and HD samples. Note the two *y* axes: left is the bulk and LD samples reciprocal χ_{HF} and right is the HD reciprocal χ_{HF}. (b) First derivative of the reciprocal of χ_{HF} for the bulk, LD, and HD samples plotted on an arbitrary scale.

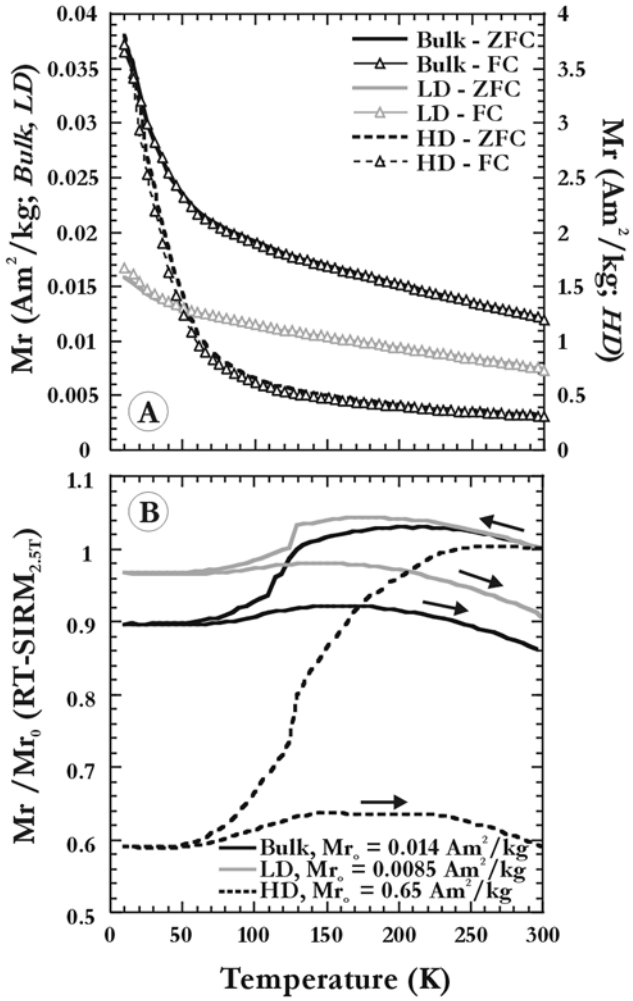

Figure 8. (a) Measurement of the temperature dependence of the saturation isothermal remanent magnetization (SIRM) acquired in 2.5 T at 10 K upon warming under two different initial conditions. The bulk, LD, and HD samples were either cooled from 300 K to 10 K in a 2.5 T magnetic field (FC) or in zero magnetic field (ZFC). Note the two *y* axes: left is for the bulk and LD samples remanence and right is for the HD remanence. (b) Normalized SIRM acquired in 2.5 T at 300 K is cycled from 300 K to 10 K and back again to 300 K for the bulk, LD, and HD samples.

titanium-rich end-member). A similar equation derived from the data of *Nagata and Akimoto* [1956] and from other sources is published by *Hunt et al.* [1995]. Titanium poor phases, TH0 (or hematite) through TH50, display slightly imperfect antiferromagnetism. The phases between TH50 and TH80 have been the most studied because of their ability to exhibit strong ferrimagnetism (for TH70 M_S is one third to a half of magnetite's saturation magnetization of 92 A m^2/kg) as well as the ability of self-reversing its magnetization. However, this ferrimagnetic property is highly dependent on the highest temperature from which the phase cooled [*Hoffman*, 1975; *Nord and Lawson*, 1989]. Magnetic properties of titanium-rich phases, TH80 to TH100 (or ilmenite), have been less studied because at room temperature they are paramagnetic. However, long-range magnetic ordering does occur at lower temperatures. For example, end-member ilmenite is antiferromagnetic below ~63 K, its Néel temperature. The studies by *Ishikawa* [1962], *Shirane et al.* [1962], *Ishikawa et al.* [1985], *Arai et al.* [1985], *Arai and Ishikawa* [1985], *Brown et al.* [1993], and *McEnroe et al.* [2002] are, to our knowledge, the only studies specifically targeted at analyzing the magnetic properties through low-temperature experiments of phases with titanium contents greater than 80%.

[21] From both magnetization experiments and neutron scattering analyses these aforementioned studies have constructed a magnetic phase diagram (Figure 13 of *Ishikawa et al.* [1985] redrawn in Figure 2 of *McEnroe et al.* [2002]) in which high titanium ilmenite-hematite series phases ($y > 0.7$) exhibit spin glass properties below their spin glass freezing temperature (T_g; $\leq$~40 K) and antiferromagnetism, superparamagnetism and/or ferrimagnetism above T_g and below T_N or T_C, respectively, as titanium content decreases. The spin glass state, based on our current understanding, is broadly defined by randomly orientated magnetic moment vectors possessing a certain statistical distribution of magnetic moment magnitudes [*Rancourt*, 2001]. The "random" configuration results from competing positive and negative magnetic exchange interactions producing frustrated magnetic spin moments [*Moorjani and Coey*, 1984]. Because of a limited variety of compositions involved in the study by *Ishikawa et al.* [1985] (TH90, TH83, and TH79), the drawn boundaries of the magnetic phase diagram are incomplete. We should also note that the compositions of the synthetic single crystals were indirectly determined by assuming a linear relationship (Vegard's law) between the volume of a unit cell (measured by X-ray analysis) and the composition. This assumption contradicts the work of others who concluded that the relationship was not linear and that such an assumption would underestimate of the titanium content [*Hoffman*, 1975; *Lawson*, 1981; *Lindsley*, 1965]. A maximum underestimation of ~7% would be incurred for mid-range compositions while the effect would decrease for approaching end-member compositions. In the present study, given that the samples are of natural origin and that the TH phase coexists with three TM phases, it is difficult to determine whether the TH phase in the OC tephra behaves as predicted by the magnetic phase diagram proposed by *Ishikawa et al.* [1985].

[22] The ilmenite-hematite series phase in the Old Crow tephra clearly undergoes a final magnetic ordering transition to paramagnetism at elevated temperatures where we observe a peak in χ' data (210 K, Figures 3 (left), 4 (left), and 5b), a loss of low-field hysteresis in χ'' data (220 K, Figures 3 (right) and 4 (right)) and an inflection point in strong field induced magnetization (230 K, Figures 6 and 7). Our best estimate of this ordering temperature is determined from the coercivity versus temperature data of the bulk sample plotted in Figure 9. At 230 K, the ilmenite-hematite series phase, which following equation (3) corresponds to TH81, becomes paramagnetic. However, whether the transition is a Curie temperature (i.e., ferrimagnetism to paramagnetism) or a Néel temperature (i.e., imperfect antiferromagnetism to paramagnetism) is not clear based on the data presented in section 4.1. There is no remanence fluctuation across the ordering temperature (Figure 8),

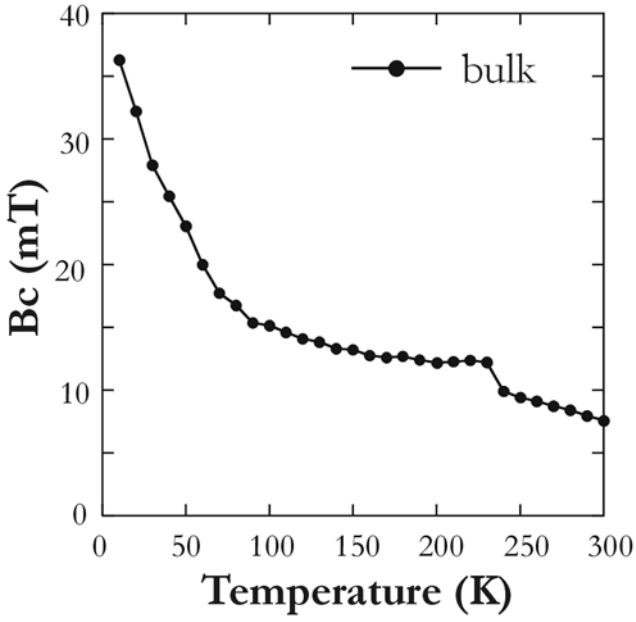

Figure 9. Temperature dependence of the bulk sample's coercivity determined from low-temperature hysteresis loops measured every 10 K from 10 K to 300 K.

supporting a purely antiferromagnetic behavior. In this case the χ' peak at 210 K in the low-field experiments (Figures 3, 4, and 5) would mark T_N and we would expect B_C to drop off at 210 K, which we do not observe (Figure 9). Instead, B_C abruptly reduces by ~3 mT at 230 K (Figure 9) which marks the same ordering temperature suggested by high-field experiments (Figures 6 and 7). Moreover the amplitude of the ordering transition decreases with increasing applied fields (Figure 6) so much that it is no longer detectable in the LD sample and only detectable in the bulk sample after some data processing (Figures 6 and 7). If we assume that the ordering temperature is a Curie point at 230 K, the χ' peak at 210 K may be similar to a Hopkinson peak but the lack of covariance between B_C and χ' remains a puzzle.

[23] We conclude that high titanium phases of the ilmenite-hematite series which magnetically disorder to paramagnetism below room temperature can be quickly and effectively recognized in natural samples, even in low concentration as is the case in the bulk and LD samples, by measuring the frequency and field dependence of the in-phase and quadrature components of susceptibility.

4.2.2. Magnetite-Ulvöspinel Series Phase

[24] The high-temperature thermomagnetic experiment on the bulk sample (see section 4.1.1 and Figure 2) clearly identifies three T_C at 395°C, 518°C, and 584°C, which we attribute to ~TM30, ~TM10, and a more or less pure magnetite or TM0. Compositions corresponding to identified T_C were determined by using the second-order polynomial equation best fitting published T_C data reported by *Hunt et al.* [1995]. The preheating and postheating hysteresis loops (Figure 2c) indicate that the sample suffered minor alteration indicated by increases in saturation and remanent magnetization as well as coercivity. The increase in M_S after heating corresponds to a production of 0.006% by mass assuming TM0 or 0.008% by mass assuming TM10. The oxidation of titanomagnetite would increase T_C, while reduction would decrease T_C [see *Hunt et al.*, 1995, Figure 8]. Even though the binding agent used to cement the sample onto the high-temperature resistant holder can create local reducing experimental environments, it is expected that oxidation also occurs locally. Minor oxidation increasing the oxidation parameter z from 0.0 to ~0.1 would be sufficient to increase T_C by ~20°C [*Hunt et al.*, 1995, Figure 8]. Oxidation would also lead to an increase in coercivity (Figure 2).

[25] The hysteresis loops (Figure 1) were measured at room temperature; therefore only (titano)magnetite phases contribute to M_S. Using equation (1) and assuming that the saturation magnetization of magnetite, TM10, and TM30 are approximately 92, 81, and 60 A m^2/kg, respectively, we can evaluate the mass percentage of the (titano)magnetite population in the LD, HD, and bulk samples. The HD sample has an M_S of 8.4 A m^2/kg; therefore the (titano)-magnetite population represents between 9% and 14% of the sample mass, depending on the proportions of the three phases (i.e., 9% if all magnetite and 14% if all TM30). Similarly in the LD sample the (titano)magnetite population represents between 0.05% (all magnetite) and 0.08% (all TM30) of the sample mass. Given that the bulk sample is composed of 0.62% HD material and 99.38% LD material, we can determine that the bulk sample's (titano)magnetite population represents between 0.11% (all magnetite) and 0.17% (all TM30) of the total sample mass.

[26] The room temperature (RT) hysteresis loops (Figure 1) and derived parameters (Table 2) characterize the HD sample population as having multidomain-type behavior (M_R/M_S = 0.076; B_{CR}/B_C = 4.09) and the LD sample population as having pseudosingle-domain-type behavior (M_R/M_S = 0.220; B_{CR}/B_C = 2.47) [*Day et al.*, 1977; *Dunlop and Özdemir*, 1997]. The RT-SIRM experiment (Figure 8b) demonstrates that magnetite is present in both the LD and HD separated fractions. Moreover, the HD sample suffers a 40% remanence loss on cooling and subsequently warming through T_V compared to only 9% remanence loss by the LD sample. For stoichiometric magnetite remanence losses, under the same experimental conditions as in this study, of ~15% for 0.037 μm grains, ~20% for 0.1 μm grains, and ~55% for 0.22 μm grains have been reported [*Özdemir et al.*, 2002]. The behavior for titanomagnetite RT-SIRM during cycling to low temperature is not well documented in the literature. However, the temperature dependence of its LT-SIRM is observed to follow the temperature dependence of the anisotropy constant [*Kakol et al.*, 1991; *Moskowitz et al.*, 1998], and the Verwey transition in single crystals is suppressed with a Ti content as little as 0.4% [*Kakol et al.*, 1994]. Therefore RT-SIRM results in Figure 8b clearly demonstrate the presence of stoichiometric multidomain magnetite in the HD sample and magnetite particles that are more oxidized or much finer in the LD sample. The lack of a Verwey transition in the low-temperature (LT) SIRM experiments (Figure 8a) is somewhat puzzling. The suppression of T_V in the LD sample may be related to a grain-size distribution that straddles the SP–SSD boundary although neither hysteresis data nor $\chi'(f, T)$ appear to indicate the dominance of such an assembly. In the HD sample the lack of an observable Verwey transition leads us to believe that the concentration of TM0 is extremely low with respect

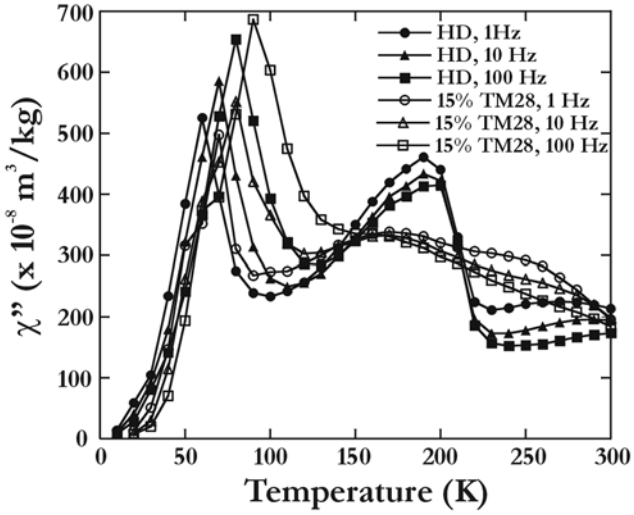

Figure 10. Superimposed quadrature susceptibility data of the HD sample shown in Figure 3 (right) and the quadrature susceptibility equivalent to a TM28 concentration of 15% by mass. The experimental settings are the same with the exception of the maximum amplitude of the AC field (240 A/m for HD and 200 A/m for TM28). The TM28 multidomain single crystal belongs to the same sample suite studies of *Moskowitz et al.* [1998] and *Jackson et al.* [1998].

to the TM10 and especially TM30 (see below) and TH81 concentrations. The remanence behavior of all four phases contributes to the LT-SIRM results (Figure 8a), while the TH81 phase is excluded from the RT-SIRM experiments since it is paramagnetic at room temperature. The 77% remanence loss suffered by 65 K in the HD sample during the LT-SIRM experiments is a combined expression of TM10, TM30 and TH81 remanence behavior which for the titanomagnetite phases is related to the significant temperature dependence of their anisotropy and magnetostriction constants [*Moskowitz et al.*, 1998]. The synthetic single and polycrystalline samples of *Moskowitz et al.* [1998] in the compositional range between TM05 to TM41 all lost large fractions (50–90%) of their low-temperature remanence below 65 K.

[27] On the basis of ongoing unpublished research at our laboratory and published studies [*Jackson et al.*, 1998; *Moskowitz et al.*, 1998; *Radhakrishnamurthy and Likhite*, 1993; *Worm and Jackson*, 1999], the temperature, frequency (Figure 3), and field (Figure 4) dependence of AC susceptibility between 30 K and 90 K predominantly reflects the behavior of titanomagnetite as well as superparamagnetic particles in the LD sample. From equation (2) we can determine that the quadrature susceptibility up to 70 K results from magnetic relaxation. Similar behavior is observed in synthetic multidomain TM28. We have modeled temperature dependence of the quadrature component of susceptibility for a 15% by mass contribution of TM28, based on AC susceptibility measurements of the TM28 multidomain single crystal studied by *Moskowitz et al.* [1998] and *Jackson et al.* [1998]. In Figure 10, the model results are superimposed on the HD χ'' data shown in Figure 3 (right). The correlation provides strong evidence that in our HD sample TM30 is the dominant phase of the magnetite-ulvöspinel series phases present. At the present time we do not have an explanation for the cause of the frequency dependence of AC susceptibility variations observed between 30 K and 90 K; however, they appear very characteristic of titanomagnetites [*Radhakrishnamurthy and Likhite*, 1993] and potentially useful as magnetic indicators. Above 70 K low-field hysteresis and magnetic relaxation both contribute to χ''. This is true for both the LD and HD even though the shape and amplitude of the low temperature peak in χ'' differ in the two density fractions. Low-temperature experiments such as $\chi(f, \mathrm{H}, \mathrm{T})$ can be just as useful in the identification of TM phases as demonstrated earlier for titanium-rich titanohematite.

5. Application to Tephra Bed Identification

[28] Tephra deposits are excellent indicator beds and have facilitated stratigraphic correlations in marine, lacustrine and terrestrial depositional environments. When sufficiently thick and unaltered, tephra layers are easily identifiable in the sediment column. However, when tephra layers are thin or dispersed due to diagenesis/pedogenesis, they may go unnoticed. Moreover, heavy alteration of the primary grains may result in resistant glass and its inclusions being the only remnants left of the original tephra layer. We have demonstrated in this study that careful low-temperature rock magnetic experiments can identify tephras by characterizing the very low concentrations of Fe-Ti oxides. These minerals are routinely used in tephrochronology, along with glass compositions, in order to correlate tephra beds within a region.

[29] At the Halfway House loess deposit, four tephra beds have been identified [*Preece et al.*, 1999], but all except the thick Old Crow tephra have gone unnoticed by others [*Begét*, 1990; *Begét and Hawkins*, 1989; *Begét et al.*, 1990; *Lagroix and Banerjee*, 2002; *Oches et al.*, 1998]. The SD tephra was observed ~3 m above the Old Crow tephra "in a dark silt sequence that has been deformed by solifluction" [*Preece et al.*, 1999], but the tephra is thin (~1 mm) and discontinuous (J. A. Westgate, personal communication, 2003). With low-temperature frequency- and field-dependent measurements of the in-phase and quadrature components of magnetic susceptibility we have identified, within a bulk sample of loess (96HH1-8.10m), Fe-Ti oxides that we believe belong to the SD tephra, given that the stratigraphic location is consistent with the observations of *Preece et al.* [1999]. These oxides have been dispersed and are found within bulk sediment spanning 10 cm depth of the profile. Figure 11 shows the $\chi(f, \mathrm{T})$ data of sample 96HH1-8.10m, where the low concentration of tephra material dispersed within the loess requires that the paramagnetic contribution be removed from the in-phase component (Figure 11, top) in order to observe the peak in χ' at 150 K (Figure 11, middle). In the quadrature component, a frequency-independent (Figure 11, bottom) and amplitude-dependent (not shown) peak at 140 K is clearly observable and unambiguous, corresponding to low-field hysteresis of a titanohematite phase with composition of approximately TH90.

6. Conclusions

[30] The mineralogy of the Fe-Ti oxide population of the Old Crow tephra is composed of four phases: TM0, TM10,

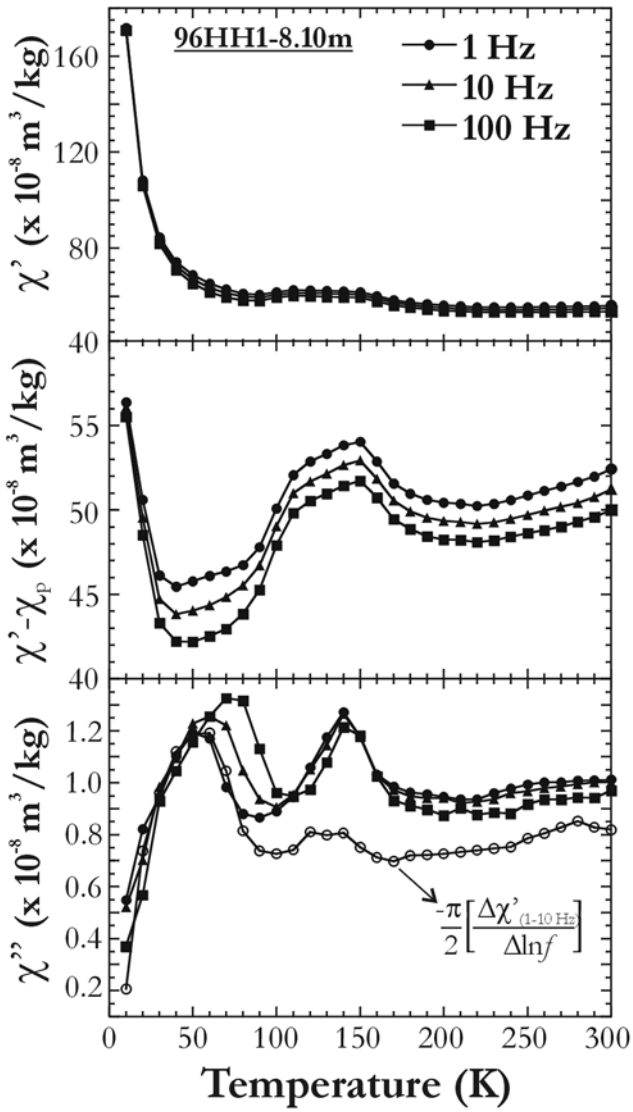

Figure 11. (top) In-phase and (bottom) quadrature components of magnetic susceptibility measured between 10 K and 300K in a constant 240 A/m field amplitude and at seven frequencies (1, 3, 10, 30, 100, 300, and 1000 Hz; not all shown) for sample 96HH1-8.10m. (middle) Paramagnetic component subtracted from the in-phase susceptibility in order accentuate the variability due only to the 90% Ti ilmenite-hematite series phase present in low concentration in the sample.

TM30 and TH81. Of these four phases TH81 and TM30 are by far the most abundant. The compositions of the magnetite-ulvöspinel series phases were best determined from the second derivative of the thermomagnetic experiment (Figure 1) which identified Curie temperatures at 395°C, 518°C, and 584°C corresponding to TM30, TM10, and TM0, respectively. The titanohematite phase was most easily identified through low-temperature frequency- and field-dependent AC magnetic susceptibility experiments. However, our best estimate of the temperature of its magnetic disordering to paramagnetism (230 K) comes from the temperature dependence of coercivity and high-field experiments conducted at low temperature, and it corresponds to TH81. Our magnetic mineralogical phase analysis independently confirms the results obtained by *Westgate et al.* [1985] identifying TM28 and TH81 using microprobe analytical techniques and additionally identified two other magnetite-ulvöspinel series phases, magnetite and TM10. In our rock magnetic analysis we were able to sample a greater population of grains and one that is unbiased by grain-size aliasing, resulting in the identification of four Fe-Ti oxide phases.

[31] The heavy liquid (2850 kg/m^3) separation of the bulk OC tephra sample into a high-density (HD) sample and a low-density (LD) sample permitted the concentration of the Fe-Ti oxide population. The low-temperature $\chi(f, T)$ experiments (Figure 3) confirm that the TH81 and titanomagnetite phase(s) are present in small amounts in LD and highly concentrated in HD sample (~15% of TM28 by mass in HD sample) and the RT-SIRM experiment (Figure 8b) convincingly identifies magnetite in both samples. While the HD sample is characterized by coarser multidomain (titano)-magnetite, the oxide population within the LD sample appears finer grained, and more oxidized. Within the LD sample, the Fe-Ti oxides are dominant as inclusions within the glass shards and other silicates. Therefore we conclude that the Fe-Ti oxide phases present in the LD and HD sample are identical in composition.

[32] A low-temperature rock magnetic approach, given some prior knowledge of the probable location of a tephra bed, is shown here to be useful and rapid to execute and we believe it has the potential to increase our ability for regional correlation of sedimentary deposits in all types of environments (i.e., marine, lacustrine, and terrestrial). Furthermore, titanium-rich phases (ilmenite content >80%) of the ilmenite-hematite series are a common primary mineral in numerous igneous rocks [*Frost and Lindsley*, 1991]. In the field of rock magnetism, titanohematite phases with more than 80% ilmenite have been somewhat neglected because of their paramagnetic state at room temperature, which renders them useless for recording the direction and intensity of the Earth's magnetic field. However, as the applications of rock magnetism become more interdisciplinary, there is a realization of the need for accurate means of identifying and quantifying the complete magnetic mineral assemblage. As presented here, a combined approach of high- and low-temperature experiments in weak and strong magnetic fields can fill the role of characterizing magnetic mineral phases and their grain size.

[33] **Acknowledgments.** We thank B. Carter-Stiglitz for help with the heavy liquid separation. The manuscript was reviewed by an anonymous reviewer, A. Hirt, Ö. Özdemir, and L. Tauxe. Support was provided by the University of Minnesota Department of Geology and Geophysics and the Geological Society of America Student Research grant 7189-02 awarded to F. Lagroix. This is contribution 0308 of the Institute for Rock Magnetism, which is funded by the W. M. Keck Foundation, the Earth Sciences Division of the National Science Foundation, and the University of Minnesota.

References

Ade-Hall, J. M., R. L. Wilson, and P. J. Smith (1965), The petrology, Curie points and natural magnetization of basic lavas, *Geophys. J.*, *9*, 323–336.

Arai, M., and Y. Ishikawa (1985), A new oxide spin glass system of $(1 - x)FeTiO_3 - xFe_2O_3$. III. Neutron scattering studies of magnetization in a cluster type spin glass of $90FeTiO_3 - 10Fe_2O_3$, *J. Phys. Soc. Jpn.*, *54*(2), 795–802.

Arai, M., Y. Ishikawa, N. Saito, and H. Takei (1985), A new oxide spin glass system of $(1 - x)FeTiO_3 - xFe_2O_3$. II. Neutron scattering studies of a cluster type spin glass of $90FeTiO_3 - 10Fe_2O_3$, *J. Phys. Soc. Jpn.*, *54*(2), 781–794.

Begét, J. E. (1990), Middle Wisconsinan climate fluctuations recorded in central Alaskan loess, *Geogr. Phys. Quat.*, *44*(1), 3–13.

Begét, J. E., and D. B. Hawkins (1989), Influence of orbital parameters on Pleistocene loess deposition in central Alaska, *Nature*, *337*, 151–153.

Begét, J. E., D. B. Stone, and D. B. Hawkins (1990), Paleoclimate forcing of magnetic susceptibility variations in Alaskan loess during the late Quaternary, *Geology*, *18*(1), 40–43.

Berger, G. W., B. J. Pillans, and A. S. Palmer (1992), Dating loess up to 800 ka by thermoluminescence, *Geology*, *20*(5), 403–406.

Brown, N. E., A. Navrotsky, G. L. Nord, and S. K. Banerjee (1993), Hematite-ilmenite ($Fe_2O_3 - FeTiO_3$) solid solutions: Determinations of Fe-Ti order from magnetic properties, *Am. Mineral.*, *78*, 941–951.

Day, R., M. Fuller, and V. A. Schmidt (1977), Hysteresis properties of titanomagnetites: Grain-size and compositional dependence, *Phys. Earth Planet. Inter.*, *13*, 260–267.

Deer, W. A., R. A. Howie, and J. Zussman (1966), *An Introduction to Rock-Forming Minerals*, 528 pp., Addison-Wesley-Longman, Reading, Mass.

Dunlop, D. J., and Ö. Özdemir (1997), *Rock Magnetism*: *fundamentals and frontiers*, 573 pp., Cambridge Univ. Press, New York.

Fournelle, J. H., B. D. Marsh, and J. D. Myers (1994), Age, character, and significance of Aleutian arc volcanism, in *The Geology of North America*, vol. G1, *The Geology of Alaska*, edited by G. Plafker and H. C. Berg, pp. 723–757, Geol. Soc. of Am., Boulder, Colo.

Froese, D., J. Westgate, S. Preece, and J. Storer (2002), Age and significance of the late Pleistocene Dawson tephra in eastern Beringia, *Quat. Sci. Rev.*, *21*, 2137–2142.

Frost, B. D., and D. H. Lindsley (1991), Occurrence of iron-titanium oxides in igneous rocks, in *Oxide Minerals*: *Petrologic and Magnetic Significance*, *Rev. Mineral.*, vol. 25, edited by D. H. Lindsley, pp. 433–468, Mineral. Soc. of Am., Washington, D. C.

Grommé, G. S., T. L. Wright, and D. L. Peck (1969), Magnetic properties and oxidation of iron-titanium oxide minerals in Alae and Makaopuhi lava lakes, *J. Geophys. Res.*, *74*, 5277–5294.

Hamilton, T. D., and J. Brigham-Grette (1991), The last interglaciation in Alaska: Stratigraphy and paleoecology of potential sites, *Quat. Int.*, *10–12*, 49–71.

Hoffman, K. A. (1975), Cation diffusion processes and self-reversal of thermoremanent magnetization in the ilmenite-hematite solid solution series, *Geophys. J. R. Astron. Soc.*, *41*, 65–80.

Hunt, C. P., B. M. Moskowitz, and S. K. Banerjee (1995), Magnetic properties of rocks and minerals, in *Rock Physics and Phase Relations*: *A Handbook of Physical Constants*, *AGU Ref Shelf*, vol. 3, edited by T. J. Ahrens, pp. 189–204, AGU, Washington, D. C.

Ishikawa, Y. (1962), Magnetic properties of ilmenite-hematite system at low temperature, *J. Phys. Soc. Jpn.*, *17*(12), 1835–1844.

Ishikawa, Y., N. Saito, M. Arai, Y. Watanabe, and H. Takei (1985), A new oxide spin glass system of $(1 - x)FeTiO_3 - xFe_2O_3$. I. Magnetic properties, *J. Phys. Soc. Jpn.*, *54*(1), 312–325.

Jackson, M., B. Moskowitz, J. Rosenbaum, and C. Kissel (1998), Field-dependence of AC susceptibility in titanomagnetite, *Earth Planet. Sci. Lett.*, *157*, 129–139.

Kakol, Z., J. Sabol, and J. M. Honig (1991), Magnetic anisotropy of titanomagnetites $Fe_{3-x}Ti_xO_4$, $0 \leq x \leq 0.55$, *Phys. Rev. B*, *44*, 2198–2204.

Kakol, Z., J. Sabol, J. Stickler, A. Kozlowski, and J. M. Honig (1994), Influence of titanium doping on the magnetocrystalline anisotropy of magnetite, *Phys. Rev. B*, *49*, 12,767–12,772.

Lagroix, F., and S. K. Banerjee (2002), Paleowind directions from the magnetic fabric of loess profiles in central Alaska, *Earth Planet. Sci. Lett.*, *195*, 99–112.

Lawson, C. A. (1981), Magnetic and microstructural properties of minerals of the ilmenite-hematite solid solution series with special reference to the phenomenon of reverse thermoremanent magnetism, Ph.D. dissertation, Princeton Univ., Princeton, N. J.

Lide, D. R. (2002), *CRC Handbook of Chemistry and Physics*, 83rd ed., CRC Press, Boca Raton, Fla.

Lindsley, D. H. (1965), *Iron-Titanium Oxides*, pp. 144–148, Carnegie Inst. of Washington, Washington, D. C.

McEnroe, S. A., R. J. Harrison, P. Robinson, and F. Langenhorst (2002), Nanoscale haematite-ilmenite lamellae in massive ilmenite rock: An example of 'lamellar magnetism' with applications for planetary magnetic anomalies, *Geophys. J. Int.*, *151*, 890–912.

Miller, T. P., and D. H. Richter (1994), Quaternary volcanism in the Alaska Peninsula and Wrangell Mountains, Alaska, in *The Geology of North America*, vol. G1, *The Geology of Alaska*, edited by G. Plafker and H. C. Berg, pp. 759–779, Geol. Soc. of Am., Boulder, Colo.

Moorjani, K., and J. M. D. Coey (1984), *Magnetic Glasses*, 525 pp., Elsevier Sci., New York.

Moskowitz, B. M. (1981), Methods for estimating Curie temperatures of titanomagnetites from experimental Js-data, *Earth Planet. Sci. Lett.*, *53*, 84–88.

Moskowitz, B. M., M. Jackson, and C. Kissel (1998), Low-temperature magnetic behavior of titanomagnetites, *Earth Planet. Sci. Lett.*, *157*, 141–149.

Mullins, C. E., and M. S. Tite (1973), Magnetic viscosity, ouadrature susceptibility, and frequency dependence of susceptibility in single-domain assemblies of magnetite and maghemite, *J. Geophys. Res.*, *78*, 804–809.

Nagata, T., and S. Akimoto (1956), Magnetic properties of ferromagnetic ilmenites, *Geofis. Pura Appl.*, *34*, 36–50.

Néel, M. L. (1949), Théorie du trainage magnétique des ferromagnétiques en grains fins avec applications aux terres cuites, *Ann. Geophys.*, *5*(2), 99–136.

Nord, G. L., and C. A. Lawson (1989), Order-disorder transition-induced twin boundaries and magnetic properties in ilmenite-hematite, *Am. Mineral.*, *74*, 160–176.

Oches, E. A., S. K. Banerjee, P. A. Solheid, and M. Frechen (1998), High-resolution proxies of climate variability in the Alaska loess record, in *Dust Aerosols, Loess Soils and Global Change* (*Extended Abstracts*), edited by A. Busacca, pp. 167–170, Wash. State Univ., Pullman.

Özdemir, Ö., D. J. Dunlop, and B. Moskowitz (2002), Changes in remanence, coercivity and domain state at low temperature in magnetite, *Earth Planet. Sci. Lett.*, *194*, 343–358.

Plafker, G., and H. C. Berg (1994), Overview of the geology and tectonic evolution of Alaska, in *The Geology of North America*, vol. G1, *The Geology of Alaska*, edited by G. Plafker and H. C. Berg, pp. 989–1022, Geol. Soc. of Am., Boulder, Colo.

Preece, S. J., J. A. Westgate, B. A. Stemper, and T. L. Péwé (1999), Tephrochronology of late Cenozoic loess at Fairbanks, central Alaska, *Geol. Soc. Am. Bull.*, *111*(1), 71–90.

Radhakrishnamurthy, C., and S. D. Likhite (1993), Frequency dependence of low-temperature susceptibility peak in some titanomagnetites, *Phys. Earth Planet. Inter.*, *76*, 131–135.

Rancourt, D. G. (2001), Magnetism of Earth, planetary, and environmental nanomaterials, in *Nanoparticles and the Environment*, *Rev. Mineral. Geochem.*, vol. 44, edited by J. F. Banfield and A. Navrotsky, pp. 217–292, Mineral. Soc. of Am., Washington, D. C.

Shirane, G., D. E. Cox, W. J. Takei, and S. L. Ruby (1962), A study of the magnetic properties of the $FeTiO_3 - \alpha Fe_2O_3$ system by neutron diffraction and the Mossbauer effect, *J. Phys. Soc. Jpn.*, *17*, 1598–1611.

Westgate, J. A. (1982), Discovery of a large-magnitude, late Pleistocene volcanic eruption in Alaska, *Science*, *218*(4574), 789–790.

Westgate, J. A., R. C. Walter, G. W. Pearce, and M. P. Gorton (1985), Distribution, stratigraphy, petrochemistry, and paleomagnetism of the late Pleistocene Old Crow tephra in Alaska and the Yukon, *Can. J. Earth Sci.*, *22*, 893–906.

Westgate, J. A., B. A. Stemper, and T. L. Péwé (1990), A 3 m.y. record of Pliocene-Pleistocene loess in interior Alaska, *Geology*, *18*(9), 858–861.

Worm, H.-U., and M. Jackson (1999), The superparamagnetism of Yucca Mountain Tuff, *J. Geophys. Res.*, *104*, 25,415–25,425.

S. K. Banerjee, M. J. Jackson, and F. Lagroix, Institute for Rock Magnetism, Department of Geology and Geophysics, University of Minnesota, 108 Pillsbury Hall, 310 Pillsbury Drive SE, Minneapolis, MN 55455, USA. (lagr0012@umn.edu)